Attenuation of acoustic waves and mechanical vibrations at low frequencies by a nonlinear dynamical absorber

D. LAVAZEC[a,b], G. CUMUNEL[a], D. DUHAMEL[a], C. SOIZE[b]

a. Université Paris-Est, Laboratoire Navier, ENPC/IFSTTAR/CNRS, 6 et 8 Avenue Blaise Pascal, Cité Descartes, Champs-sur-Marne, 77455 Marne La Vallée Cedex 2, France
b. Université Paris-Est, Laboratoire Modélisation et Simulation Multi Echelle, MSME UMR 8208 CNRS, 5 bd Descartes, 77454 Marne-la-Vallée, France
Email : deborah.lavazec@univ-paris-est.fr

Résumé :

À l'heure actuelle, l'atténuation des ondes acoustiques et des vibrations mécaniques en moyennes et hautes fréquences est bien connue et facilement réalisable, en particulier avec des matériaux dissipatifs. Cependant, cette atténuation est beaucoup plus difficile à réaliser en basses fréquences en raison des grandes longueurs d'onde. Dans le travail présenté ici, nous proposons de réduire le bruit et les vibrations en basses fréquences sur une large bande de fréquences au moyen d'absorbeurs non-linéaires permettant un transfert et une dissipation de l'énergie. Ces absorbeurs sont répartis aléatoirement dans une matrice et ont un comportement dynamique non-linéaire. L'absorbeur se compose d'une poutre encastrée-libre supportant une masse concentrée à son extrémité. Il est conçu pour obtenir un comportement dynamique non-linéaire dans la bande basses fréquences grâce aux déplacements finis de la poutre. Ce système mécanique est modélisé par un système masse-ressort-amortisseur avec une rigidité non-linéaire et un amortissement non-linéaire. En effet, la non-linéarité permet une atténuation sur une bande de fréquence plus large, contrairement aux systèmes linéaires qui ne génèrent qu'une réduction sur une bande de fréquences étroite autour de la résonance, ce qui permet de réduire le nombre d'absorbeurs nécessaires pour une atténuation donnée. Nous allons d'abord présenter la conception de l'absorbeur non-linéaire optimisé en utilisant une modélisation stochastique afin d'obtenir la réponse non-linéaire la plus adéquate possible. Ensuite, les résultats expérimentaux seront présentés ainsi que leurs comparaisons avec les prédictions numériques.

Abstract :

At the present time, the attenuation of acoustic waves and mechanical vibrations at high and middle frequencies is well known and easily done, especially with dissipative materials. However, this attenuation is much more difficult to realize at low frequencies because of the large wavelengths. In the work presented here, we propose to reduce the noise and the vibrations at low frequencies over a broad frequency band by means of nonlinear absorbers allowing a transfer and a dissipation of the energy. These absorbers are randomly arranged in a matrix and have a nonlinear dynamical behavior. The absorber consists of a cantilever beam supporting a concentrated mass at its end. It is designed in order to obtain a nonlinear dynamical behavior in the low-frequency band due to the finite displacements of the

beam. This mechanical system is modeled by a mass-spring-damper system with a nonlinear stiffness and a nonlinear damping. Indeed, nonlinearity allows attenuation over a broader frequency band, unlike linear systems which only generate a reduction over a narrow frequency band around the resonance, which makes it possible to reduce the number of absorbers needed for a given attenuation . We will first present the design of the nonlinear absorber optimized using stochastic modeling in order to obtain the most adequate nonlinear response possible. Then, experimental results will be presented as well as their comparisons with the numerical predictions.

Keywords : noise attenuation, vibrations attenuation, nonlinear absorber, homogeneization, metamaterial

1 Introduction

As it is well known, the reduction of acoustic waves and vibration at middle and high frequencies is mainly done by the dissipative materials. With these materials, the waves are reduced thanks to the pores of the materials. However, for the low frequencies, the wavelength are larger that the pores, and the dissipative materials are less efficient. To get around this problem, absorbers at low frequencies had been designed, in particular oscillators. Among the first papers devoted to the enery pumping by simple oscillators, the work by Frahm [1] in 1911 can be cited. The author presents the idea of a system for the damp or avoid the vibrations of a body submitted to periodic impacts with an auxiliary body. The resonance vibrations of the main body are annulled by the secondary resonance vibrations of the smaller auxiliary body. In nearer years, the tuned mass dampers have been studied. The principle is to add an oscillator (generally a mass-spring-damping system) to a main structure with a problematic resonance. The resonance frequency of the damper is calibrated in order to be the same that the structure's to attenuate the resonance. With that, the peak is divided into two peaks of low amplitudes. A review made by Gutierrez Soto et al. [2] presents a representative research on tuned mass dampers. Metamaterials had also be used for the reduction of noise and vibrations. A metamaterial is a material with properties that can not be find in nature, generally a composite. There are for instance materials with both negative permittivity and negative permeability in optic [3]. In the domain of the absorption of vibrations and noise, numerous papers have been published with metamaterials, as for instance, [4, 5, 6, 7, 8, 9, 10, 11]. In 1952, Roberson [12] have presented the equations of a nonlinear dynamic vibration absorber and highlighted the fact that a nonlinear auxiliary body offers significant advantages over a corresponding linear absorber. It has been confirmed by Soize [13] in 1995 that the transfer of the energy is done over a broader frequency band with a nonlinear auxiliary body that a linear one. Concerning the energy pumping by nonlinear mechanical oscillators in order to attenuate vibrations and noise for discrete or continuous systems at macro- or at micro-scales, many works have been published such as [14, 15, 16, 17, 18, 19, 20, 21].

This paper is devoted to the reduction of vibrations and induced noise in structures at macro-scale for the low-frequency band for which the first structural modes are excited. The final objective of this work is to reduce vibrations and induced noise on a broad low-frequency band by using a microstructured material by inclusions that are randomly arranged in the material matrix. The first step of this work is to design and to analyze the efficiency of an inclusion, which is made up of a cantilever beam with a point mass at the end. This inclusion behaves as a nonlinear oscillator that is designed in order that the energy

pumping be efficient on a broad frequency band around its resonance instead of a narrow frequency band as for a linear oscillator. For this first step, the objective is to develop the simplest mechanical model that has the capability to roughly predict the experimental results that are measured. The second step will consist in developing a more sophisticated nonlinear dynamical system. In this paper, devoted to the first step, it is proved that the nonlinearity induced an attenuation on a broad frequency band around its resonance, whereas the associated linear system yields a reduction only on a narrow frequency band. We will present the design in terms of geometry, dimension and materials for the inclusion, the experimental manufacturing of this system realized with a 3D printed system, and the experimental measures that have been performed. We compare the prevision given by the stochastic computational model with the measurements. The results obtained exhibit the physical attenuation over a broad low-frequency band, which were expected.

In Section 2, we will present the design of the model of the inclusion and the stochastic solver related. Then, in Section 3 is displayed the experimental design. The experimental measurements and the identification of the model will be also showed. In Section 4, we will conclude on the results of this work and we will describe the perspectives of the future work.

2 Design of the nonlinear model and stochastic solver

2.1 Computational model of the inclusion

As explained in Section 1, a nonlinear oscillator with one DOF is constructed for modeling the nonlinear dynamical behavior of the inclusion. The one-DOF nonlinear model is composed of a mass-spring-damper system with a nonlinear spring and a nonlinear damping, excited by its support (see the scheme displayed in Figure 1). Let $X_{\text{imp}}^{\text{exp}}(t)$ be the displacement imposed at the support in the absolute frame and let $X_s(t)$ be the relative displacement of the point mass with respect to the support. Let

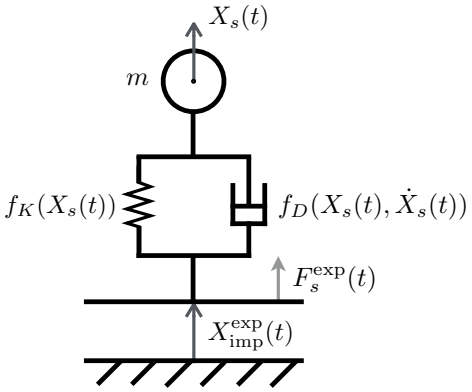

FIGURE 1 – 1D simplified model.

$\{\ddot{X}_{\text{imp}}^{\text{exp}}(t), t \in \mathbb{R}\}$ be the acceleration imposed to the support, which is a Gaussian stationary second-order centered stochastic process, defined on the probability space $(\Theta, \mathcal{T}, \mathcal{P})$, for which the power spectral density function is denoted by $S_{\ddot{X}_{\text{imp}}^{\text{exp}}}(\omega)$. We aim to find the stationary second-order stochastic solution $\{X_s(t), t \in \mathbb{R}\}$ (which is not Gaussian) of the following stochastic nonlinear equation

$m(\ddot{X}_s(t) + \ddot{X}^{\text{exp}}_{\text{imp}}(t)) + f_D(X_s(t), \dot{X}_s(t)) + f_K(X_s(t)) = 0$ for t in $\mathbb{R}$, which is rewritten as

$$m\ddot{X}_s(t) + f_D(X_s(t), \dot{X}_s(t)) + f_K(X_s(t)) = F^{\text{exp}}_s(t),\ t \in \mathbb{R}, \tag{1}$$

in which

$$\begin{aligned} F^{\text{exp}}_s(t) &= -m\,\ddot{X}^{\text{exp}}_{\text{imp}}(t)\ , \\ f_D(X_s(t), \dot{X}_s(t)) &= \big(c_1 + c_2|X_s(t)|\big)\dot{X}_s(t)\ , \\ f_K(X_s(t)) &= k_1 X_s(t) + k_3 (X_s(t))^3\ , \end{aligned}$$

where m is the mass of the inclusion introduced before, c_1 and c_2 are the damping coefficients and k_1 and k_3 are the stiffness coefficients. The nonlinear stiffness is written as a cubic nonlinearity because it is the form of nonlinearity due to geometric effects that can be observed experimentally. There is not quadratic coefficient in order to obtained a centered response since the excitation is a centered stochastic process.

The mean input power $\Pi_{\text{in}} = E\{F^{\text{exp}}_s(t)\,\dot{X}_s(t)\}$ (in which E is the mathematical expectation) and the mean power dissipated

$$\Pi_{\text{diss}} = E\{f_D(X_s(t), \dot{X}_s(t))\dot{X}_s(t)\}\ ,$$

which are independent of t and which are equal (due to the stationarity), can be written as $\Pi_{\text{in}} = \int_{\mathbb{R}} \pi_{\text{in}}(\omega)\,d\omega$ and $\Pi_{\text{diss}} = \int_{\mathbb{R}} \pi_{\text{diss}}(\omega)\,d\omega$, in which the density $\pi_{\text{in}}(\omega)$ and $\pi_{\text{diss}}(\omega)$ are such that

$$\pi_{\text{in}}(\omega) = S_{F^{\text{exp}}_s \dot{X}_s}(\omega) \quad , \quad \pi_{\text{diss}}(\omega) = S_{f_D \dot{X}_s}(\omega)\,. \tag{2}$$

In Eq. (2), $S_{F^{\text{exp}}_s \dot{X}_s}$ is the cross-spectral density function of the stationary stochastic processes F^{exp}_s and $\dot{X}_s$, and $S_{f_D \dot{X}_s}(\omega)$ is the cross-spectral density function of the stationary stochastic processes f_D and $\dot{X}_s$. The energy pumping expressed as a function of the frequency is therefore characterized by $\pi_{\text{in}}(\omega) = \pi_{\text{diss}}(\omega)$. In order to qualify the efficiency of this energy pumping as a function of the intensity of the nonlinearity, we introduce the normalized quantity,

$$\pi_{\text{in,norm}}(\omega) = \frac{\pi_{\text{in}}(\omega)}{S_{F^{\text{exp}}_s}(\omega)}\ . \tag{3}$$

Finally, the damping and stiffness coefficients will be experimentally identified by using the frequency dependent function $\text{FRF}^2(\omega)$ defined on B_0 by,

$$\text{FRF}^2(\omega) = \frac{|S_{\dot{X}_s F^{\text{exp}}_s}(\omega)|^2}{|S_{F^{\text{exp}}_s}(\omega)|^2} \tag{4}$$

It should be noted that if $f_D(x)$ and $f_K(x)$ were linear functions of x (linear oscillator), then FRF^2 would represent the square of the modulus of the frequency response function of the associated linear filter for which F^{exp}_s is the input and $\dot{X}_s$ is the output.

2.2 Stochastic solver and signal processing

Stochastic solver. For constructing the stationary stochastic solution of the nonlinear differential equation Eq. (1), the Monte Carlo method (see [22]) is used. Let $\{F^{\text{exp}}_s(t;\theta_\ell), t \in \mathbb{R}\}$ be a realization of the

stochastic process F_s^{exp} for $\theta_\ell \in \Theta$. Considering L independent realizations, for each realization θ_ℓ, we then have to solve the deterministic nonlinear differential equation with initial conditions,

$$\left\{ \begin{array}{c} m\ddot{X}(t;\theta_\ell) + f_D(X(t;\theta_\ell), \dot{X}(t;\theta_\ell)) + f_K(X(t;\theta_\ell)) = F_s^{\text{exp}}(t;\theta_\ell),\ t \in [0, t_0+T], \\ \\ X(0,\theta_\ell) = 0,\ \dot{X}(0,\theta_\ell) = 0. \end{array} \right. \tag{5}$$

The part $\{X(t;\theta_\ell), t \in [0,t_0]\}$ of the non-stationary random response corresponds to the transient signal induces by the initial conditions, that decreases exponentially due to the damping. This part of the response is removed in the signal processing of the second-order quantities of the stationary solution. Time t_0 is chosen in order that the transient response be negligible for $t \geq t_0$. The part of the trajectory corresponding to the stationary response is $X_s(t;\theta_\ell) = X(t-t_0;\theta_\ell)$ for t in $[t_0, t_0+T]$. The time duration T that is related to the frequency resolution is defined after. The deterministic problem defined by Eq. (5) will be solved with a Störmer-Verlet scheme presented after.

Time and frequency sampling. For constructing the second-order quantities of the stationary response X_s, the signal processing requires a time sampling with a constant time step Δ_t that is performed using the Shannon theorem for the stationary stochastic processes [23]. The sampling frequency is thus written as $f_e = 2\, f_{\text{max}}$ and the time step is $\Delta_t = 1/f_e$. The corresponding time sampling is $t_\alpha = \alpha\, \Delta_t$ with $\alpha = 0, 1, ..., N-1$ in which the integer N is chosen in order that the frequency resolution $\Delta_f = 1/T = 0.125\, Hz$ where $T = N\Delta_t$ yielding $N = 16,384$ for $T = 8\, s$. The corresponding sampling points in the frequency domain are $f_\beta = -f_{\text{max}} + (\beta + 1/2)\Delta_f$ for $\beta = 0, 1, ..., N-1$.

Generation of independent realizations of stochastic process F_s^{exp}. The usual second-order spectral representation of the stationary stochastic processes is used [24, 25]. The power spectral density function $S_{F_s^{\text{exp}}}(\omega)$ of the Gaussian stationary second-order centered stochastic process F_s^{exp} is such that $S_{F_s^{\text{exp}}}(\omega) = m^2\, S_{\ddot{X}_{\text{imp}}^{\text{exp}}}(\omega)$, in which $S_{\ddot{X}_{\text{imp}}^{\text{exp}}}(\omega) = \omega^4\, S_{X_{\text{imp}}^{\text{exp}}}(\omega)$. The autocorrelation function $\tau \mapsto R_{\ddot{X}_{\text{imp}}^{\text{exp}}}(\tau)$ of stochastic process $\ddot{X}_{\text{imp}}^{\text{exp}}$ is such as $R_{\ddot{X}_{\text{imp}}^{\text{exp}}}(\tau) = E\{\ddot{X}_{\text{imp}}^{\text{exp}}(t+\tau)\ddot{X}_{\text{imp}}^{\text{exp}}(t)\}$ and is such that $R_{\ddot{X}_{\text{imp}}^{\text{exp}}}(\tau) = \int_R e^{i\omega\tau} S_{\ddot{X}_{\text{imp}}^{\text{exp}}}(\omega)\, d\omega$. The generator of realizations of the Gaussian stationary second-order stochastic process $\ddot{X}_{\text{imp}}^{\text{exp}}$ is based on the usual spectral representation (see [26, 27]). Let $\Psi_0, \ldots, \Psi_{N-1}$ be N mutually independent uniform random variables on $[0,1]$, and let $\phi_0, \ldots, \phi_{N-1}$ be N mutually independent uniform random variables on $[0, 2\pi]$, which are independent of $\Psi_0, \ldots, \Psi_{N-1}$. The spectral representation used is,

$$\ddot{X}_{\text{imp}}^{\text{exp}}(t) \simeq \sqrt{2\Delta_\omega}\, \text{Re}\Big\{ \sum_{\beta=0}^{N-1} \sqrt{S_{\ddot{X}_{\text{imp}}^{\text{exp}}}(\omega_\beta)}\, Z_\beta\, e^{-i\omega_\beta t}\, e^{-i\phi_\beta} \Big\},\ t \in [0, t_0+T]\ , \tag{6}$$

in which $\Delta_\omega = 2\pi\, \Delta_f$, where $Z_\beta = \sqrt{-\log(\Psi_\beta)}$ and $\omega_\beta = 2\pi\, f_\beta$. From Eq. (6), it can be deduced that the realization $\{\ddot{X}_{\text{imp}}^{\text{exp}}(t;\theta_\ell)\, , t \in [t_0; t_0+T]\}$ is written as

$$\ddot{X}_{\text{imp}}^{\text{exp}}(t;\theta_\ell) \simeq \sqrt{2\Delta_\omega}\, \text{Re}\Big\{ \sum_{\beta=0}^{N-1} g_{\beta,\ell}\, e^{-i\omega_\beta t} \Big\},\ t \in [0, t_0+T]\, , \tag{7}$$

in which $g_{\beta,\ell} = \sqrt{S_{\ddot{X}_{\text{imp}}^{\text{exp}}}(\omega_\beta)}\, Z_\beta(\theta_\ell)\, e^{-i\phi_\beta(\theta_\ell)}$. Introducing the FFT $\{\widehat{g}_{0,\ell}, \ldots, \widehat{g}_{N-1,\ell}\}$ of $\{g_{0,\ell}, \ldots, g_{N-1,\ell}\}$,

which is written as $\widehat{g}_{\alpha,\ell} = \sum_{\beta=0}^{N-1} g_{\beta,\ell} \, \exp\{ -2i\,\pi\,\alpha\beta/N\}$ for $\alpha = 0, 1, ..., N-1$, we obtain

$$\ddot{X}^{\exp}_{\text{imp}}(t_\alpha;\theta_\ell) = \sqrt{2\Delta_\omega}\,\text{Re}\Big\{ \exp\{ -i\pi\alpha\big(\frac{1-N}{N}\big)\}\,\widehat{g}_{\alpha,\ell}\Big\}\,, \alpha = 0, 1, \ldots, N-1\,. \tag{8}$$

Störmer-Verlet integration scheme. The Störmer-Verlet integration scheme is well suited for the resolution of dynamical Hamiltonian systems [28, 29] as proposed, for instance, for the dissipative case, in [30]. Such a scheme preserves the mechanical energy during the numerical integration. We thus rewrite Eq. (5) in the following dissipative Hamiltonian form as

$$\left\{\begin{array}{l} \dot{X}(t;\theta_\ell) = \dfrac{1}{m}\,Y(t;\theta_\ell), \qquad t \in [t_0, t_0+T]\,, \\ \\ \dot{Y}(t;\theta_\ell) = -f_D(Y(t;\theta_\ell) - k_1 X(t;\theta_\ell) \\ \qquad\qquad -k_3(X(t;\theta_\ell))^3 + F^{\exp}_s(t;\theta_\ell), \qquad t \in [t_0, t_0+T]\,, \\ \\ X(0;\theta_\ell) = 0\,,\; Y(0;\theta_\ell) = 0\,. \end{array}\right. \tag{9}$$

We use the notation $u^\alpha_\ell = U(t_\alpha;\theta_\ell)$. The Störmer-Verlet integration scheme for Eq. (9) is then written, for $\alpha = 0, 1, ..., N-1$, as

$$\left\{\begin{array}{l} x^{\alpha+1/2}_\ell = x^\alpha_\ell + \dfrac{\Delta_t}{2m}\,y^\alpha_\ell\,, \\ \\ y^{\alpha+1}_\ell = y^\alpha_\ell + \Delta_t\Big[-\dfrac{f_D(y^\alpha_\ell) + f_D(y^{\alpha+1}_\ell)}{2} \\ \qquad\qquad -k_1 x^{\alpha+1/2}_\ell - k_3(x^{\alpha+1/2}_\ell)^3 + F^{\exp}_s(t_{\alpha+1};\theta_\ell)\Big]\,, \\ \\ x^{\alpha+1}_\ell = x^{\alpha+1/2}_\ell + \dfrac{\Delta_t}{2m} y^{\alpha+1}_\ell\,, \end{array}\right. \tag{10}$$

in which $F^{\exp}_s(t_{\alpha+1};\theta_\ell) = -m\ddot{X}^{\exp}_{\text{imp}}(t_{\alpha+1};\theta_\ell)$.

Signal processing. For estimating, the power spectral density functions and the cross-spectral density functions defined in Eqs. (2) and (4), the periodogram method [23] is used.

3 Experimental design choice, measurements and identification of the model

In Section 2, we defined the design of the computational model and the related stochastic solver. In this section, we want to design a experimental model that can be assimilated to a nonlinear oscillator.

Concerning the choice of the design to correspond to a nonlinear oscillator, we had several constraints. Indeed, the bulk of the inclusion has been fixed around two centimeters, in order to be in the approximated size of the biggest aggregates in concrete (supposing that the inclusion can be put in a wall of

concrete for example). In addition, we want an oscillator with a strong nonlinear behavior without big displacements to remain in the bulk define previously. Also, we need an oscillator with a weak damping to absorb the energy on a broad frequency band. After tests on different structures (these tests will be develop in a future paper), we choose to focus on a cantilever beam with a point mass at its end.

3.1 Presentation of the test structure

The inclusion has been designed at a macro-scale. It is made up of a point mass constituted of a cube, embedded at the end of a beam. The other end of the beam is attached to a frame. The beam length is $0.026\,m$ and its square section is $0.001 \times 0.001\,m^2$. The exterior dimensions of the cube are $0.008 \times 0.008 \times 0.008\,m^3$. The material of the inclusion and of the frame is in ABS. This inclusion is manufactured using a 3D printing system (the ABS (Acrylonitrile Butadiene Styrene) is commonly used as a material for 3D printing). The mass m of the inclusion is approximated by the sum of the mass of the

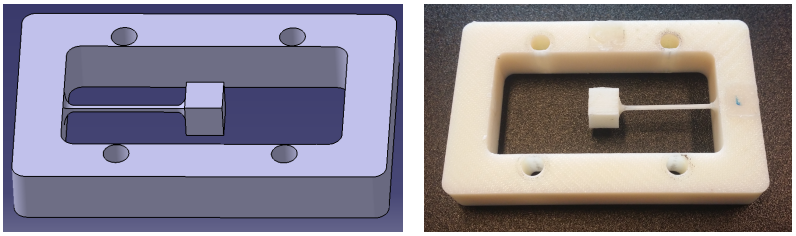

(a) CAO (b) 3D printing

FIGURE 2 – CAO and 3D printing of the test structure.

accelerometer attached to it that is $0.0004\,kg$, the mass of its cable $0.0002\,kg$ and the mass of the cube $0.00055\,kg$, so the mass m is $0.0012\,kg$ (the mass of the beam is neglected). The mass density of the ABS is $1,780\,kg/m^3$. Some experimental traction tests have been carried out for identifying the mechanical properties of the ABS material which is assumed to be homogeneous, linear elastic and isotropic. The experiments yield for the Young modulus, $2.2 \times 10^9\,Pa$ and for the Poisson coefficient 0.35. This inclusion has been designed in order that the first eigenfrequency of the frame be around $1,200\,Hz$ and the first eigenfrequency of the inclusion (point mass, accelerometer and beam) be around $24\,Hz$. We are interested in analyzing the stationary random response of the inclusion in the frequency band of analysis $B_a = [0, f_{\max}]$ with $f_{\max} = 1,024\,Hz$, induced by the stationary random excitation generated by an imposed acceleration of the embedded end of the beam. This acceleration is equal to the acceleration that is imposed to the frame (that can be considered as rigid in the frequency band of analysis), on which a stationary random external force is applied (see Section 3). The frequency band that is observed is the band $B_o = [21, 26]\,Hz \subset B_a$, which contains the resonance frequency for all amplitudes of the excitation.

3.2 Experimental results and identification of the model

The experimental configuration can be viewed in Figure 3. The acceleration $\ddot{X}^{\exp}_{\text{imp}}$ at a point of the rigid frame that is fixed and the acceleration $\ddot{X}^{\exp}$ of the point mass (inclusion) are measured with two accelerometers. The excitation applied to the rigid frame is done by a shaker. The experimental responses have been measured for seven amplitudes of the experimental accelerations $\ddot{X}^{\exp}_{\text{imp}}$. These cases will be identified by a percentage noted d/h where h is the thickness of the beam, $h = 0.001\,m$, and d is defined

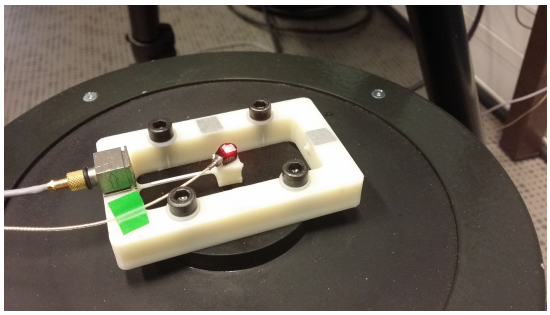

FIGURE 3 – The experimental configuration.

as

$$d = \frac{100}{2L}\Big(\sum_{\ell=1}^{L} max(X^{\exp}(t;\theta_\ell)) - \sum_{\ell=1}^{L} min(X^{\exp}(t;\theta_\ell))\Big) \ .$$

For instance, if a case is defined by $d/h = 100\%$, the displacement of the inclusion is of the order of magnitude of the thickness of the beam. The power spectral density function of the force applied to the oscillator $S_{F_s}^{\exp}$ is displayed in Figure 4 for each cases and for the frequency band B_o.

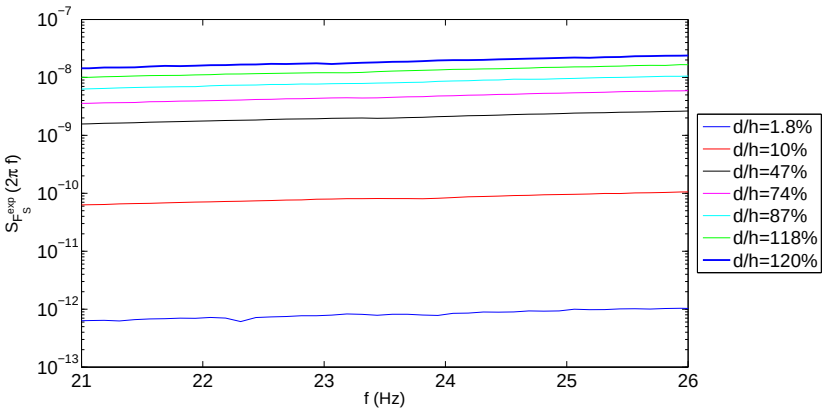

FIGURE 4 – Experimental PSD function $S_{F_x}^{exp}$ for seven amplitudes of the excitation.

As explained in Section 2.1, for all of the amplitudes, the experimental identification of the damping and stiffness parameters is performed by minimizing over the frequency band B_o, the distance between FRF^2 (defined by Eq. (5)) computed with the model and the same quantity constructed with the experimental measurements.

During the identification, we have noted that the damping of the system was non-linear, contrarily to the predictions in Section2. According to [31], the form chosen for f_D in order to keep a centered response is $f_D(X_s(t), \dot{X}_s(t)) = \big(c_1 + c_2|X_s(t)|\big)\dot{X}_s(t)$. The experimental identification gives

$$\begin{cases} k_1 = 26.8\, N/m \ , \\ k_3 = -4 \times 10^6 N/m^3 \ , \\ c_1 = 0.0038 Ns/m \ , \\ c_2 = 10 Ns/m^2 \ . \end{cases} \tag{11}$$

For each one of the seven amplitudes, Figure 5 displays the comparison of the FRF^2 function for the identified model with that obtained with the experiments. It can be seen a reasonable agreement between the experiments and the computation, knowing that an approximation has been introduced for constructing the model (see the explanations given in Section 2.1).

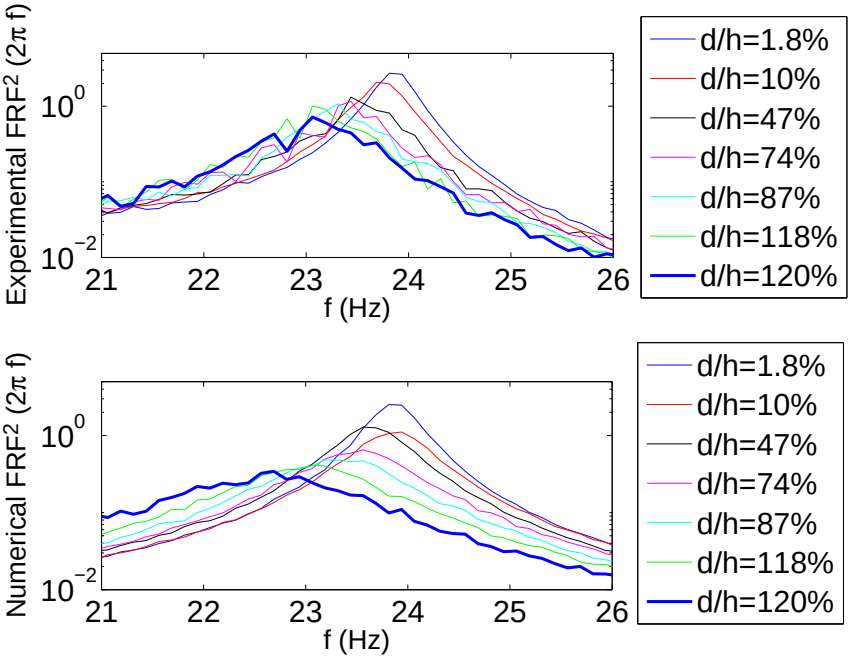

FIGURE 5 – Comparison of the experimental FRF^2 (exp) with the identified computational model (num) for the seven amplitudes.

Figure 6 display the comparison of the experimental and the numerical normalized input power density defined by Eq. (3) for the seven amplitudes. It can be seen a reasonable agreement between the prediction with the model and the experiments. Furthermore, the results presented in this figure confirm a strong effect of the nonlinearity that allows the pumping energy phenomenon to be efficient over a broader frequency band around the resonance frequency than for the linear case, which was the objective of the work.

4 Conclusions

In this paper, we have presented the results related to the first step of a work devoted to the design and the analysis of a nonlinear microstructured material to reduce noise and vibrations at low frequencies. We have developed the design of an inclusion at macroscale, which has been manufactured with a 3D printing system. The dimension of this inclusion can easily be reduced with the same technology. A first version of a nonlinear dynamical model has been developed and its parameters have been identified with the experiments. Both the predictions given by the model and the experiments confirm that the pumping energy phenomenon is more efficient over a broader frequency band around the resonance frequency than for the linear case. The work in progress is the development of a more sophisticated model of the inclusion, which takes into account the nonlinear couplings between several degrees of freedom.

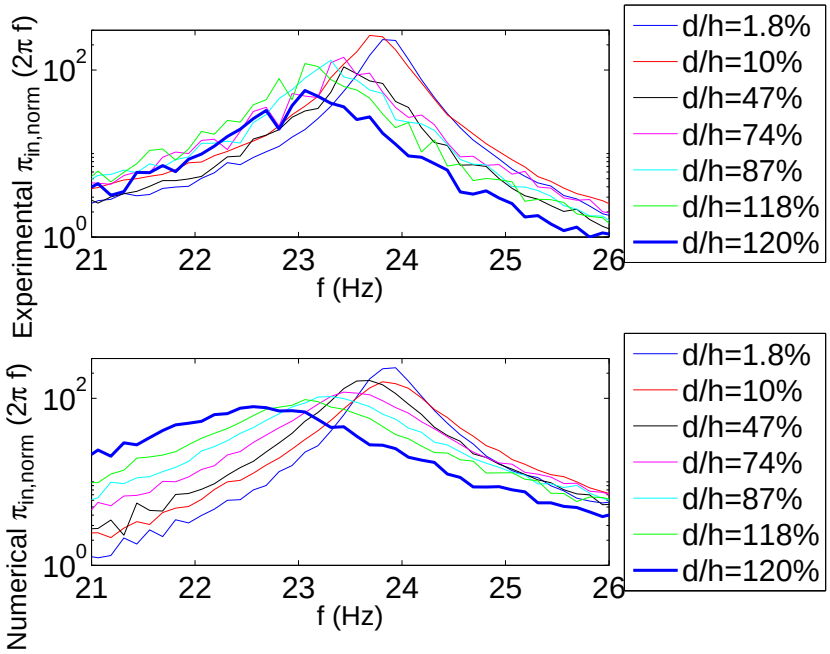

FIGURE 6 – Comparison of the experimental normalized input power density $\pi^{exp}_{\text{in,norm}}$ with the identified computational model for the seven amplitudes.

Acknowledgements

This work has benefited from a French government grant managed by ANR within the frame of the national program investments for the Future ANR-11-LABX-002-01.

References

[1] H. Frahm, Device for damping vibrations of bodies, United states patent office (1911) 1–9.

[2] M. Gutierrez Soto, H. Adeli, Tuned mass dampers, Archives of Computational Methods in Engineering 20 (4) (2013) 419–431.

[3] V. G. Veselago, The elctrodynamics of substances with simultaneously negative values of epsilon and nu, Soviet Physics 509.

[4] D. Smith, N. Kroll, Negative refractive index in left-handed materials , Physical Review Letters 85 (2000) 2933–2936.

[5] H. Chen, C. Chan, Acoustic cloaking in three dimensions using acoustic metamaterials, Applied Physics Letters 91 (2007) 183518–1, 183518–3.

[6] Z. Yang, J. Mei, M. Yang, N. Chan, P. Sheng, Membrane-type acoustic metamaterial with negative dynamic mass, Physical Review Letters 101(20) (2008) 204301–1, 204301–4.

[7] X. Zhou, G. Hu, Analytic model of elastic metamaterials with local resonances, Physical Review B 79 (2009) 195109–1, 195109–9.

[8] X. Liu, G. Hu, G. Huang, C. Sun, An elastic metamaterial with simultaneously negative mass density and bulk modulus, Applied Physics Letters 98 (2011) 251907.

[9] D. Del Vescovo, I. Giorgio, Dynamic problems for metamaterials : Review of existing models and ideas for further research, International Journal of Engineering Science 80 (2014) 153–172.

[10] R. Zhu, X. Liu, G. Hu, C. Sun, G. Huang, A chiral elastic metamaterial beam for broadband vibration suppression, Journal of Sound and Vibration 333 (2014) 2759–2773.

[11] X. Wang, H. Zhao, X. Luo, Z. Huang, Membrane-constrained acoustic metamaterials for low frequency sound insulation, Applied Physics Letters 108(4) (2016) 041905.

[12] R. E. Roberson, Synthesis of a nonlinear dynamic vibration absorber, Portions of a dissertation submitted to the Department of Applied Mechanics, Washington University, in partial fulfillment of the requirements for the degree of Doctor of Philosophy. (1952) 205–220.

[13] C. Soize, Vibration damping in low-frequency range due to structural complexity. A model based on the theory of fuzzy structures and model parameters estimation, Computers and Structures 58 (1995) 901–915.

[14] O. Gendelman, L. Manevitch, A. Vakakis, R. MĆloskey, Energy pumping in nonlinear mechanical oscillators : part I-dynamics of the underlying hamiltonian systems, Journal of Applied Mechanics 68 (2001) 34–41.

[15] A. Vakakis, O. Gendelman, Energy pumping in nonlinear mechanical oscillators : part II-resonance capture, Journal of Applied Mechanics 68 (2001) 42–48.

[16] A. Vakakis, Shock isolation through the use of nonlinear energy sinks, Journal of Vibration and Control 9 (2003) 79–93.

[17] G. Milton, M. Briane, J. Willis, On cloaking for elasticity and physical equations with a transformation invariant form, New Journal of Physics 8 (2006) 1–20.

[18] A. Carrella, M. Brennan, T. Waters, Static analysis of a passive vibration isolator with quasi-zero-stiffness characteristic, Journal of Sound and Vibration 301 (2007) 678–689.

[19] Z. Yang, H. Dai, N. Chan, G. Ma, P. Sheng, Acoustic metamaterial panels for sound attenuation in the 50-1000 Hz regime, Applied Physics Letters 96 (2010) 041906–1, 041906–3.

[20] Y. Xiao, J. Wen, X. Wen, Sound transmission loss of metamaterial-based thin plates with multiple subwavelength arrays of attached resonators, Journal of Sound and Vibration 331 (2012) 5408–5423.

[21] L. Viet, N. Nghi, On a nonlinear single-mass two-frequency pendulum tuned mass damper to reduce horizontal vibration, Engineering Structures 81 (2014) 175–180.

[22] R. Rubinstein, D. Kroese, Simulation and the Monte Carlo Method, Second Edition, John Wiley & Sons, 2008.

[23] A. Papoulis, Probability, Random Variables and Stochastic Processes, McGraw-Hill, New York, 1965.

[24] L. Guikhman, A. Skorokhod, The Theory of Stochastic Processes, Springer Verlag, 1979.

[25] M. Priestley, Spectral Analysis and Time Series, Academic Press, New York, 1981.

[26] M. Shinozuka, Simulation of multivariate and multidimensional random processes, Journal of the Acoustical Society America 49 (1971) 357–367.

[27] F. Poirion, C. Soize, Numerical methods and mathematical aspects for simulation of homogeneous and non homogeneous Gaussian vector fields, in : P. Krée, W. Wedig (Eds.), Probabilistic Methods in Applied Physics, Springer-Verlag, Berlin, 1995, pp. 17–53.

[28] L. Verlet, Computer "experiments" on classical fluids. I. Thermodynamical properties of Lennard-Jones molecules, Physical Review 159 (1) (1967) 98–103.

[29] E. Hairer, C. Lubich, G. Wanner, Geometric numerical integration illustrated by the Störmer/Verlet method, Acta Numerica 12 (2003) 399–450.

[30] C. Soize, I. E. Poloskov, Time-domain formulation in computational dynamics for linear viscoelastic media with model uncertainties and stochastic excitation, Computers and Mathematics with Applications 64 (11) (2012) 3594–3612.

[31] C. Desceliers, C. Soize, Non-linear viscoelastodynamic equations of three-dimensional rotating structures in finite displacement and finite element discretization, International Journal of Non-Linear Mechanics 39 (2004) 343–368.